Online-Journals.org

iJOE International Journal of Online and Biomedical Engineering

iJOE | eISSN: 2626-8493 | Vol. 20 No. 10 (2024) | OPEN ACCESS

https://doi.org/10.3991/ijoe.v20i10.47157

PAPER

Statistical Analysis of Features for Detecting Leukemia

Vandana S. Khobragade[1](✉), Jagannath H. Nirmal[2], Aayesha Hakim[2]

[1]Lokmanya Tilak College of Engineering, Navi Mumbai, Maharashtra, India

[2]K.J. Somaiya College of Engineering, Mumbai, Maharashtra, India

vandanakhobragade@ltce.in

ABSTRACT

In this age of digital microscopy, image processing, statistical analysis, categorization, and systems for decision-making have become essential tools for medical diagnostics research. By visualizing and analyzing images, clinicians can identify anomalies in intracellular structure. Leukemia is a cancerous condition marked by an unregulated increase in aberrant white blood cells (WBCs). Recognizing acute leukemia tumor cells in blood smear images (BSI) is a challenging assignment. Image segmentation is regarded as the most significant step in the automated identification of this disease. The innovative concavity-based segmentation algorithm is employed in this study to segment WBC in sub-images from the ALLIDB2 database. The concave endpoints and elliptical features are used in the segmentation step of convex-shaped cell images. The procedure involves the extraction of contour evidence, which detects the visible section of each object, and contour estimation, which corresponds to the final object's contours. Following the identification of the cells and their internal structure by concavity-based segmentation, the cells are categorized based on their morphological and statistical features. The method was evaluated using a public dataset meant to test classification and segmentation approaches. The statistical tool SPSS is used to independently check the significance of derived features. For classification, significant features are passed into machine learning techniques such as support vector machines (SVM), k-nearest neighbor (KNN), neural networks (NN), decision trees (DT), and Nave Bayes (NB). With an AUC of 98.9% and a total accuracy of 95%, the neural network model performed better. We advocate using the neural network model to identify acute leukemia cells based on its accuracy.

KEYWORDS

acute lymphoblastic leukaemia, neural networks (NN), white blood cells (WBCs), concavity-based segmentation, machine learning, t-test

1 INTRODUCTION

The bone marrow, which fills the bone's central cavity, is where all the blood cells are produced. Stem cells develop into particular blood cells [1], such as WBCs. It is also referred to as leukocytes, which are an important part of the immune system that defends against bacteria, viruses, and other foreign substances. The five

Khobragade, V.S., Nirmal, J.H., Hakim, A. (2024). Statistical Analysis of Features for Detecting Leukemia. *International Journal of Online and Biomedical Engineering (iJOE)*, 20(10), pp. 130–150. https://doi.org/10.3991/ijoe.v20i10.47157

Article submitted 2023-12-04. Revision uploaded 2024-02-04. Final acceptance 2024-02-05.

subcategories of leukocytes are neutrophils, monocytes, eosinophils, basophils, and lymphocytes [2]. However, the immune system is impacted by the cancerous production of irregular and undeveloped leukocytes, which reduces the capacity of the bone marrow to generate RBCs and platelets [3]. The condition known as leukemia is characterized by the growth of leukocytes, or blasts, in the bone marrow and blood.

While chronic leukemia can be lymphocytic or myelogenous and is marked by slow progression, acute leukemia causes the patient to rapidly degrade. However, because abnormal leukocytes quickly spread through the bloodstream and affect other body organs, a leukemia diagnosis at an earlier stage is essential [4]. Early detection of leukemia has always been a difficulty for investigators, physicians, and hematologists. Leukemia symptoms include lymph node swelling, pallor, a high fever, and a decrease in weight; however, these might additionally be associated with other illnesses.

Blood smear images have been examined in [5] and [6] for diagnosing, separating, and counting the cells in numerous types of leukemia. [7] conducts a similar type of automatic investigation, including the implementation of a unique method for diagnosing types of diabetic retinopathy. Numerous studies using image processing techniques to diagnose leukemia and segment WBCs have been published in this field [8]. This can make it easier for pathologists and hematologists to quickly diagnose leukemia and start the patient on the right course of treatment. The acquisition of images from leukemia patients is the initial stage in the automated diagnosis of leukemia. These images may be impacted by imaging-related noise, artifacts, and poor contrast. As a result, pre-processing is done to improve the quality of the acquired datasets.

The background and foreground pixels are then separated using segmentation methods based on their distinct qualities, such as color, texture, and shape [9–11]. Extensive research has been conducted to develop prospective automated leukemia detection systems [12]. Pre-processing, a method used to get rid of undesirable components from the images, is a crucial step in medical image processing [13]. This can be implemented by applying various basic as well as advanced image processing and machine vision techniques. Thus, it becomes one of the most important measures to improve the accuracy of diagnostic systems [14].

In this study, the Min-Max method of normalization is used to enhance the efficacy of the process. Image segmentation is a key component in automated disease diagnosis systems [15, 16]. According to Zuva et al. [17], shape segmentation techniques are classified into three groups: threshold-based, edge-based, and region-based. The simplest segmentation methods have traditionally been regarded as thresholding and clustering [18, 19]. Objects that do not have overlapping boundaries are suitable for thresholding [18]. Other blood cell segmentation techniques employed are thresholding and the watershed algorithm [19]. According to Chen et al. [19], the distance transform produces good results with the watershed segmentation algorithm. Gharaibeh et al. [20] proposed a novel Swin Transformer-based Segmentation using a modified U-Net and Generative Adversarial Network (ST-MUNet) algorithm. This was an example of incorporating deep learning into segmentation. The outline of the proposed paper is as follows: In Section 2, the proposed nucleus extrication from the WBC image and statistical feature extraction are elaborated. In Section 3, statistical tests of the significance of features are discussed. In Section 4, the classification methods are discussed in detail. Discussion about the results is carried out in Section 5, followed by a conclusion in Section 6.

2 METHODS AND MATERIALS

ALL-IDB [21] and ASH [22] are two of the most commonly used databases. The ALL-IDB database, which is used in this work, contains annotated (by oncologists) blood cell images. The images in the datasets were all captured with a Canon PowerShot G5 camera and saved in JPG (Joint Photographic Experts Group) format with a color depth of 24 bits. The photos correspond to different microscope magnifications (300 to 500). This database is available in two forms (ALL-IDB1 and ALL-IDB2), both of which are free and based on segmentation and categorization. The ALL-IDB2 image set was designed to assess the precision of classification. ALL-IDB2 includes cropped areas of interest for blast and normal cells from the ALL-IDB1 dataset. There are 260 images in total, with lymphoblasts accounting for half of them. The dataset is freely available to the public. If the significant cell is a blast, the images in the ALL-IDB2 dataset are labeled "ImABC 1.jpg" and "ImABC 0.jpg" in the other cases. The framework of the proposed work is as shown in Figure 1.

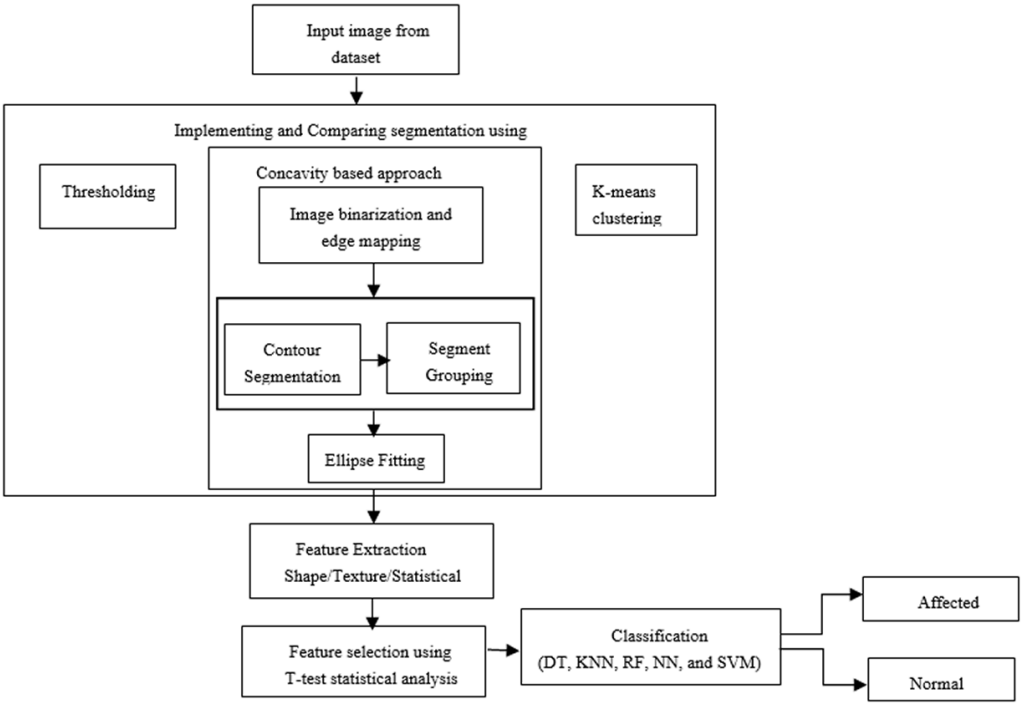

Fig. 1. Framework of proposed work

Contribution of the proposed work

1. Pre-processing and segmentation of the nucleus region segmented from the WBC/leukocyte region from the entire blood smear image (carrying platelets, RBCs) to examine the area of interest that depicts an abnormality. Use of thresholding, k-means, and concavity-based segmentation to study abnormalities.
2. Check the similarity of the segmented region with ground truth (GT) images.
3. Geometry, texture, and statistical feature extraction from concavity-based segmented ROI
4. Abnormality analysis by statistical significance of features
   I. Histogram analysis
   II. Q-Q plot analysis
5. Checking the significance of selecting features using t-test statistical analysis.

6. Classification using machine learning models, NNs, and CNN. Use feature selection to achieve a high-performance ML/AI predictive model for leukemia detection.
   - The neural network model performed better, with an AUC of 98.9% and an overall accuracy of 95%. Based on its accuracy, we recommend utilizing the neural network model to distinguish between each category of acute leukemia cells.
   - ANNs (AUC: 0.989) and Random Forest (AUC: 0.973) have the highest area values under ROC. The DT technique produced the lowest results (AUC: 0.891).

2.1 Nucleus extraction from WBC images

As already stated, image segmentation is a key component in many medical image analysis systems [23–24]. In leukemia detection, it is accomplished by distinguishing the nucleus from the cytoplasm of the cell [25]. Thresholding, region growing, watershed segmentation, and morphological segmentation are the conventional methods for differentiating the area of interest from BSIs. In this work, concave points and ellipse characteristics are used to segment images of convex-shaped cells. Here, three segmentation methods are implemented on the ALLIDB-2 database [26], namely thresholding, the proposed concave-based approach, and the color-based K-means clustering approach. The proposed approach to segmentation is discussed in detail in [27]. To distinguish the WBC from the remaining components of BSI, the detection of concave points along with segment grouping is performed. The results for the same are shown in Figure 2.

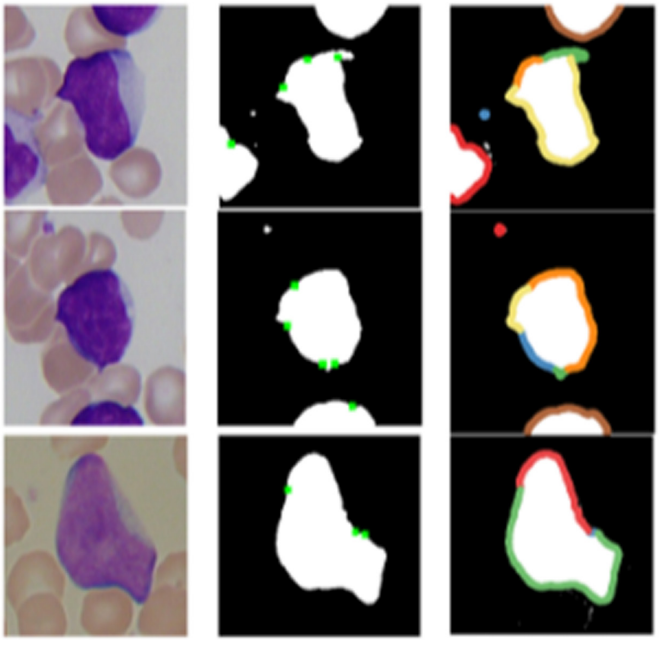

Fig. 2. Corner detection and segment grouping

2.2 Statistical feature extraction

It is the dimensionality reduction phase, in which datasets are characterized by definite sets of values. These values are unique and important for recognition

and classification. Geometrical, color-based, statistical, and many other types of features are used in leukemia detection [28–29]. The features extricated during this particular stage are utilized in the following phase to detect and classify leukemia. The accuracy of leukemia detection is completely dependent on the features used for classification. Most of the prior work on ALL detection involved the use of features extracted from the entire image. However, localization is critical for the diagnosis of abnormalities. Images are huge amounts of data to process; hence, extracted features from segmented nuclei of WBC are used for classification. By analyzing the normal and abnormal WBC images for intensity distributions, it is possible to predict the presence of an abnormality and categorize them into normal and abnormal. Figure 3 [a–p] shows the abnormality analysis by statistical significance of features using a histogram. It is observed that features are more correlated for normal cases and less correlated for abnormal patients. Among all the statistical features computed, mean, contrast, energy, skewness, kurtosis, and homogeneity remain at the same level as in a normal BSI, while these values show variation in abnormal blood smear images.

Statistical features: First-order statistics

Mean: It signifies the average color in the image.

$$Mean = m_1 = \sum_{X=0}^{N_g-1} XP(X) \tag{1}$$

Variance: Indicates the measure of the deviation between grey levels and the mean value

$$Variance = \mu_v = \sum_{X=0}^{N_g-1} (X-m)^2 P(X) \tag{2}$$

Skewness: Evaluates the asymmetry of a pixel distribution near the mean value.

$$Skewness = \mu_s = \frac{1}{\sigma^3} \sum_{X=0}^{N_g-1} (X-m)^3 P(X) \tag{3}$$

Statistical features: Second-order statistics

Kurtosis: It describes the peak of the distribution when compared to a normal distribution. It is defined as follows:

$$Kurtosis = \mu_k = \frac{1}{\sigma^4} \sum_{X=0}^{N_g-1} (X-m)^4 P(X) \tag{4}$$

Texture features: The spatial relationship of the image pixels is given by the grey-level co-occurrence matrix (GLCM). From this, the second-order statistics are derived. Here, $P(i, j)$ is the normalized GLCM value at coordinates i and j, the number of distinct grey levels is given by N_g also σ_x, σ_y and μ_x, μ_y represents the standard deviation and mean values of the normalized GLCM matrix, respectively [30].

If a pair of pixels is considered, then the grey level variation between these pairs is given by contrast. In other words, contrast is used to count the total number of local variances in the GLCM. It is given by the following equation:

$$Contrast = f_1 = \sum_{i=0}^{N_g-1}\sum_{j=0}^{N_g-1}(i-j)^2 P(i.j) \tag{5}$$

The linear dependency of the grey level value is represented by the correlation in the GLCM. It is given by following the formula in (6).

$$Correlation = f_2 = \sum_{i=0}^{N_g-1}\sum_{j=0}^{N_g-1}\frac{((i\times j)\times P(i.j)-\{\mu_x\times\mu_y\}}{\sigma_x\times\sigma_y} \tag{6}$$

The local textural uniformity of gray levels is given by the following equation. An image with a similar gray level will have a high energy value.

$$Energy = f_3 = \sum_{i=0}^{N_g-1}\sum_{j=0}^{N_g-1}p(i,j)^2 \tag{7}$$

Homogeneity: It describes the distribution of elements with regard to the GLCM's diagonals.

$$Homogenity = f_4 = \sum_{i=0}^{N_g-1}\sum_{j=0}^{N_g-1}\frac{P(i.j)}{1+(i-j)^2} \tag{8}$$

Entropy is nothing but the measure of randomness or complexity present in an image.

$$Entropy = \sum_{i=0}^{N_g-1}\sum_{j=0}^{N_g-1}p(i.j)\log(p(i,j)) \tag{9}$$

The X-axis of Figure 3 represents the number of healthy or sick BSIs, and the Y-axis shows the feature values of each individual image. The statistical analysis of four geometric features, namely area, perimeter, major axis, and minor axis, is shown in Figures 3a–3d. From the analysis, it is found that among the geometric statistical features, area and perimeter show better discriminating ability than the rest of the geometric features. From the analysis, it is found that among the first-order statistical features—mean, variance, and skewness—shown in Figures 3i, 3m, and 3p, respectively, skewness shows the best discriminating ability among the rest of the first-order statistical features. The second-order statistical feature, namely kurtosis, as shown in Figure 3o, can differentiate the normal BSI from the abnormal BSI efficiently. Similarly, the histogram of texture features, namely contrast, correlation, energy, homogeneity, and entropy, is shown in Figures 3e, 3f, and 3k. It is observed that correlation can differentiate the normal BSIs from the abnormal BSIs better than the rest. Thus, from the geometric, statistical first and second orders, and texture feature-based asymmetry analysis of the BSIs, the following observations are made:

1. Histogram analysis plays a crucial role in the abnormality detection of BSIs and shows the variations in the normal and abnormal BSIs.
2. Among all the geometric features computed, area and perimeter illustrate a noticeable difference between the normal and abnormal histograms of these features.
3. Among all the first-order statistical features computed, skewness does illustrate a noticeable difference between the normal and abnormal histograms.

4. The computed second-order statistical feature, kurtosis, also shows significant differences between the normal and abnormal histograms. This is also a good, significant biomarker for sick versus normal ones.
5. Similarly, among all the texture features computed, correlation illustrates a noticeable difference between the normal and abnormal histograms.

3 STATISTICAL TESTS FOR THE SIGNIFICANCE OF FEATURES

3.1 Setting up the hypothesis

Question: Is there a difference between normal and abnormal samples in BSIs?

Null Hypothesis: Normal and abnormal samples cannot be separated into different classes.

Alternative Hypothesis: There is a difference between normal and abnormal samples.

3.2 Test of Gaussian nature with quantile-quantile plot

In this work, 16 statistical features are extricated from the segmented WBC of BSI. The distribution of the data plays an important role in determining the classification accuracy. As per the central limit theorem, the features possess a normal distribution as they are the result of the superposition of many random processes. The SPSS statistics software is used to test the Gaussian nature of the dependent features to see if they follow a Gaussian distribution. The quantile-quantile plot in Figures 4a–4p shows the comparison of sample and theoretical quantiles of features for a normal distribution. For a feature (X) possessing a normal distribution, its quantile plot will be closer to linear.

3.3 Selecting and running an appropriate test

Geometric or morphological features, namely, area, perimeter, major axis, and minor axis; texture features, namely, contrast, correlation, energy, homogeneity, mean, std_dev, entropy, RMS, variance, smoothness, kurtosis, and skewness, are extracted from the segmented nucleus region. Since the extracted features satisfy the normality test, a parametric approach to test the significance of the data is selected. Further, as our extracted features are numeric, unpaired data, we are looking for the difference between the normal and abnormal classes; hence, the T-test for checking the significance of features becomes the best choice. Pearson's correlation can be used to check the correlation between the classes. The implications of these features are tested using the T-test in the IBM SPSS statistical tool.

In order to assess the difference between the abnormal and normal groups, the p-value, which indicates significance, is checked. In T-test, an analysis of group statistics and an independent sample test are done, and the same is shown in Tables 1 and 2, respectively. Here, the analysis is only for area features. A similar kind of discussion can be framed for other features as well. The mean area of the abnormal class is greater than that of the normal class. This shows a significant difference between the two classes.

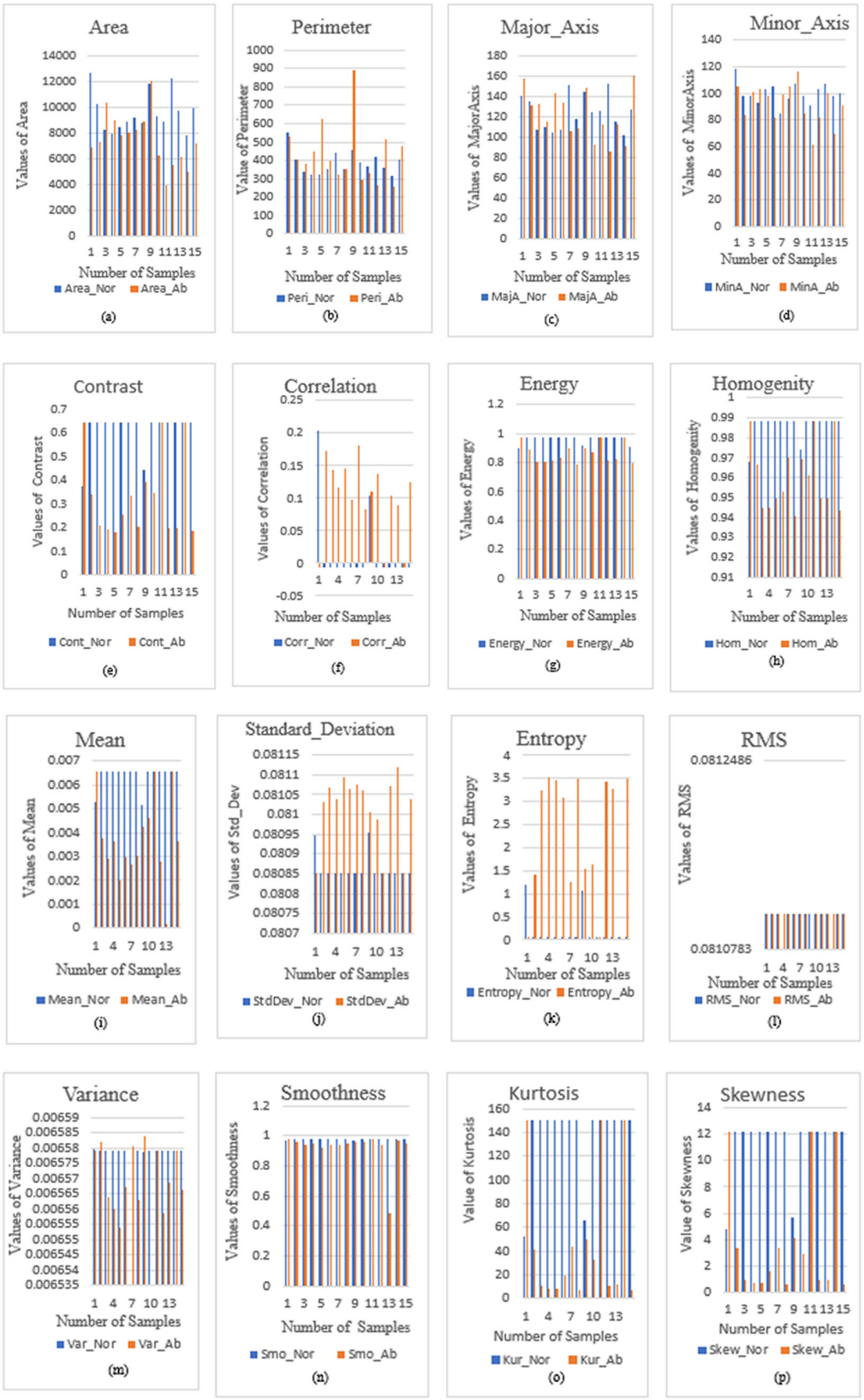

Fig. 3. Histogram analysis for features from the nucleus of concavity-based segmentation

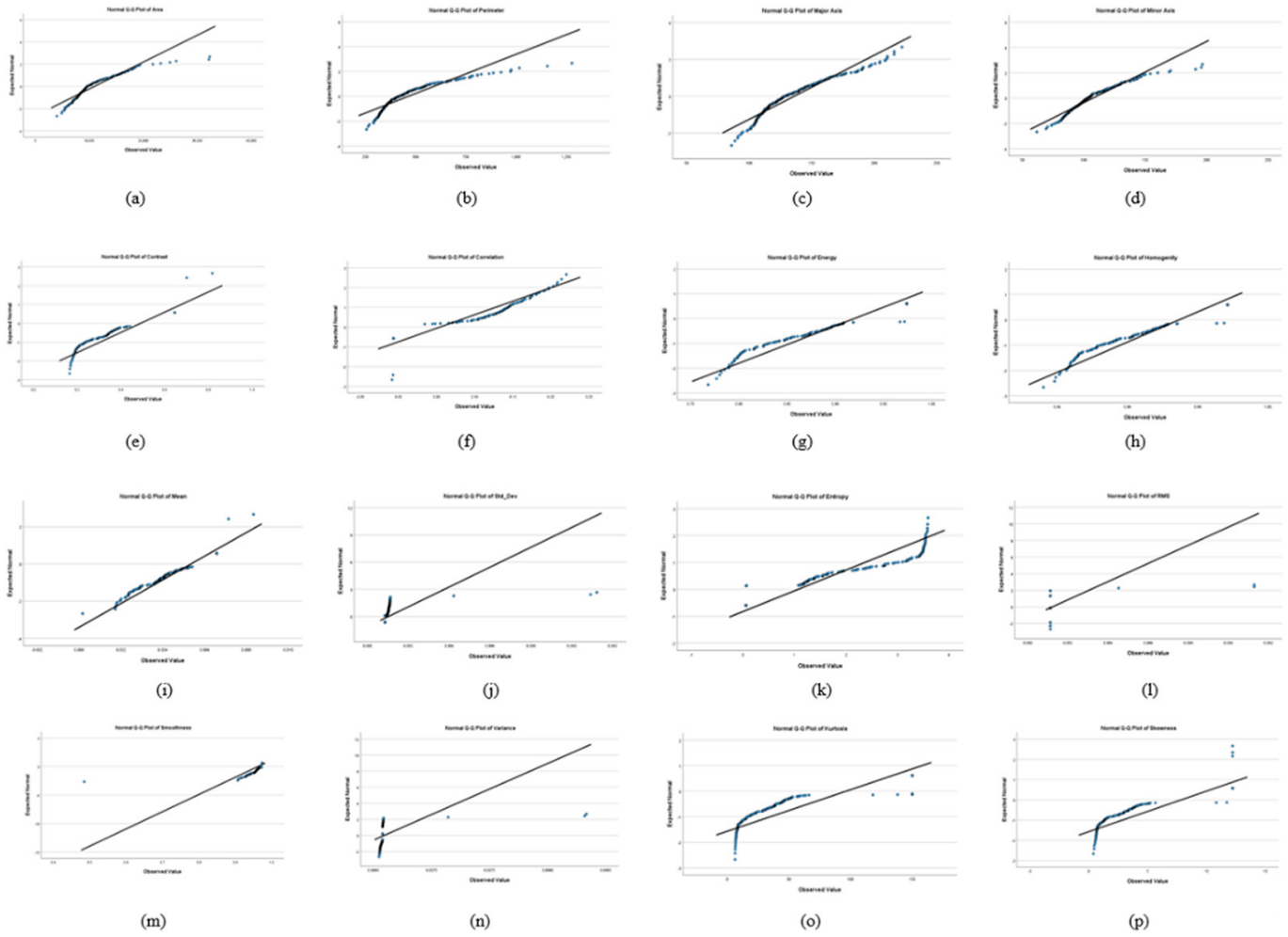

Fig. 4. Q-Q plots comparing the sample quantiles of features to the theoretical quantiles of a normal distribution

To assess the significance of the difference, the significance, or 'P' value, is considered. As both significance values are the same (<0.001), Levene's test for equality of variance will be used. In this case, the value of significance is 0.529, which is greater than 0.05. This means there is equal variance between the two classes. So, the p value used is 0.001, and it indicates that there is a significant difference in area features between the abnormal and normal classes. An independent sample T-test was conducted to compare the area for abnormal and normal groups. There was a significant difference (DF = 258) (t = 3.712) (p = < = 0.001) in the scores, with the mean score for the abnormal case (mean = 1184131, std dev = 3593965) being greater than the mean score of the normal class (mean = 9980.08, std dev = 4446.192). The magnitude of the difference in the means = 1861.223 and the 95% confidence interval (low = 0.214 and high = .706) is significant. Hence, an alternative hypothesis is selected, which says that the abnormal and normal classes differ from each other.

As represented in bold in Table 3, all the p-values that are less than 0.05 are significant, as they indicate that there is a difference between the two groups. In this manner, significant features are selected and applied to various classifiers. For statistical analysis, Statistical Package for the Social Sciences (SPSS; IBM Corp., Armonk, NY, US) 30-day student's version software is used. BSI values of $p < 0.05$ are significant. It helps to find 12 statistically prominent features (out of a total of 16 features).

4 CLASSIFICATION USING MACHINE LEARNING METHODS

For faster predictions, effective classification methodologies play a very important role. Each image has 12 significant biostatistical features. So, a set of 12×260 features are available. The Orange Analytics tool is used for implementing machine learning-based classifiers. For all algorithms, the complete data set is divided into training and test sets in the ratio of 80:20. The training data teaches the classifier the relationship between characteristics and outcomes, while the test data evaluates the classifier's generalization ability. In the field of automated medical analysis, classification can be divided into supervised and unsupervised classes. In contrast to the work mentioned in [31], which addresses an unsupervised machine learning model for detecting and analyzing DNA damage, supervised learning is frequently used to classify leukemia. This is achieved by utilizing labeled data to train the model and new data to test the model [32].

Various traditional supervised learning techniques, including SVM [33–35], NB [36–38], KNN [39–41], and ANN [42–44], are experimented with to classify leucocytes into two different classes. In a unique method proposed by Hegde et al. [45], the researchers initially segmented the WBCs before using SVM to categorize WBC cells. Using BSIs, Zhao, Jianwei, et al. [46] came up with a unique method for segmenting and categorizing leukocytes. To categorize WBCs into their five subclasses, segmentation, which is based on color correlation and the morphology of the WBC, is experimented with [47]. The WBC classification was the subject of a hybrid approach presented by Abdulkadir Sengür et al. [48]. A computer-aided diagnosis approach was suggested by Tantikitti S et al. [49] to identify dengue fever disease.

To segregate leukocytes in BSI, a multi-level threshold approach is applied. For classification, this study used two DT phases. In the first phase, categorization of WBCs as lymphocytes or phagocytes is achieved, and in the second phase, the presence of dengue virus is determined. In [50], a novel technique for segmenting the WBC nucleus and cytoplasm using simple thresholding is proposed. Following segmentation, morphological operations such as elliptical curve fitting are performed, followed by feature extraction. The sequential forward selection strategy is employed for feature selection, and a NB classifier is used to categorize WBCs. In [51], a novel technique to classify objects is proposed. This method will utilize a basic and robust geometrical model to categorize the observed object in the images as human or non-human.

Table 1. Group statistics

Feature	Target	N	Mean	Std. Deviation	Std. Error Mean
Area	1	130	1184131	3593965	315212
	0	130	9980.08	4446.192	389.957
Perimeter	1	130	440.11365	135.559278	11.889335
	0	130	488.96155	176.010601	15.437151
Major Axis	1	130	135.56178102	24.993070502	2.1920372911
	0	130	136.43794921	32.200950420	2.8242101795
Minor Axis	1	130	112.85639418	18.874031602	1.6553620773
	0	130	102.13291044	21.134227911	1.853594407

(Continued)

Table 1. Group statistics *(Continued)*

Feature	Target	N	Mean	Std. Deviation	Std. Error Mean
Contrast	1	130	0.51872469636	0.16386367793	0.01437179528
	0	130	0.45821981762	0.20168625695	0.01768905490
Correlation	1	130	.04942080101	.07420143094	.00650789601
	0	130	.05880629311	.07176767233	.00629444125
Energy	1	130	.93279638619	.05547012858	.00486505211
	0	130	.90709761045	.07398853911	.00648922416
Homogeneity	1	130	.97787670967	.01419914125	.00124534707
	0	130	.97159073053	.01853755686	.00162585129
Mean	1	130	.00559853204	.00133040094	.00011668388
	0	130	.00507636619	.00174291203	.00015286350
Std_Dev	1	130	.08091356563	.00008229906	.00000721811
	0	130	.08112358682	.00128461236	.00011266796
Entropy	1	130	.81650917333	1.0753275064	.09431246129
	0	130	1.3207128599	1.4408043292	.12636689912
RMS	1	130	.08111071057	.00000000000	.00000000000
	0	130	.08129346041	.00128909536	.00011306114
Variance	1	130	.00657748102	.00000497965	.00000043674
	0	130	.00660541009	00022175598	.00001944929
Smoothness	1	130	.96677969551	01128077206	.00098938916
	0	130	.95736161194	.04508499956	.00395421604
Kurtosis	1	130	105.13888932	56.985487013	4.9979578369
	0	130	86.981146092	64.610527424	5.6667181209
Skewness	1	130	8.5899972836	4.6035255046	.40375589609
	0	130	7.1077148053	5.2537145971	.46078125186

Table 2. Independent sample test

Features	Levene's Test for Equality of Variance			t	df	t-Test for Equality of Means			
						Significance		Mean Difference	Std. Error Difference
		F	Sig.			One-Sided p	Two-Sided p		
Area	Equal variance assumed	0.397	0.529	3.712	258	<0.001	<0.001	1861.23	501.423
	Equal variance not assumed			3.712	247.13	<0.001	<0.001	1861.23	501.423
Perimeter	Equal variance assumed	11.165	<0.001	–2.507	258	0.006	0.013	–48.847900	19.484915
	Equal variance not assumed			–2.507	242.20	0.006	0.013	–48.847900	19.484915
Major Axis	Equal variance assumed	4.828	0.029	–0.245	258	0.403	0.807	–.87616818	3.5750791
	Equal variance not assumed			–0.245	243.03	0.403	0.807	–.87616818	3.5750791

(Continued)

Table 2. Independent sample test *(Continued)*

Features	Levene's Test for Equality of Variance			t	df	t-Test for Equality of Means			Std. Error Difference
						Significance		Mean Difference	
		F	Sig.			One-Sided p	Two-Sided p		
Contrast	Equal variance assumed	32.065	<0.001	2.655	258	0.004	0.008	0.0605048	0.0227914
	Equal variance not assumed			2.655	247.62	0.004	0.008	0.0605048	0.0227914
Correlation	Equal variance assumed	.071	.790	–1.037	258	.150	.301	–.0093854921	.00905387768
	Equal variance not assumed			–1.037	257.71	.150	.301	–.0093854921	.00905387768
Energy	Equal variance assumed	29.062	<.001	3.169	258	<.001	.002	.02569877574	.00811041073
	Equal variance not assumed			3.169	239.19	<.001	.002	.02569877574	.0081104107
Homogeneity	Equal variance assumed	27.533	<.001	3.069	258	.001	.002	.00628597	.0020479945
	Equal variance not assumed			3.069	241.60	.001	.002	.00628597	.002047994
Mean	Equal variance assumed	20.590	<.001	2.715	258	.004	.007	.00052216	.0001923080
	Equal variance not assumed			2.715	241.22	.004	.007	.00052216	0001923080
Std_Dev	Equal variance assumed	6.552	.011	–1.860	258	.032	.064	–.00021002	.0001128989
	Equal variance not assumed			–1.860	130.05	.033	.065	–.0002100	.0001128989
Entropy	Equal variance assumed	25.484	<.001	–3.198	258	<.001	.002	–.50420368	.1576814305
	Equal variance not assumed			–3.198	238.68	<.001	.002	–.50420368	.1576814305
RMS	Equal variance assumed	10.810	.001	–1.616	258	.054	.107	–.00018274	.00011306114
	Equal variance not assumed			–1.616	129.00	.054	.108	.00018274	.0001130611
Variance	Equal variance assumed	9.696	.002	–1.436	258	.076	.152	–.00002792	.0000194541
	Equal variance not assumed			–1.436	129.13	.077	.154	–.0000279	0000194541
Smoothness	Equal variance assumed	6.924	.009	2.311	258	.011	.022	.00941808	.0040761152
	Equal variance not assumed			2.311	145.08	.011	.022	.00941808	.0040761152
Kurtosis	Equal variance assumed	26.080	<.001	2.403	258	.008	.017	18.157743	7.555876971
	Equal variance not assumed			2.403	254.03	.008	.017	18.157743	7.555876971
Skewness	Equal variance assumed	28.228	<.001	2.419	258	.008	.016	1.4822824	.6126485009
	Equal variance not assumed			2.419	253.62	.008	.016	1.4822824	.6126485009

4.1 Performance evaluation criteria

This section is about the performance indicators that various researchers use to assess the viability of a certain approach. The technique that can determine whether

a blast is present in a BSI is dependent on whether the blast cell was correctly classified or not. As a result, the quantity of sick cells correctly identified as positive by the test is known as True Positives (TP). The number of cells that the test correctly identifies as negative can be used to determine True Negatives (TN). False Positive (FP) denotes the proportion of cells the test defines as positive but which are actually negative, and False Negative (FN) is the proportion of elements that the test labels as negative but are actually positive. These measures can be calculated as shown in (10–13) where $Segment_{img}$ is the image segmented, and $GroundTruth_{img}$ is the image ground truth.

Table 3. Test of significance: T-test

Features	Abnormal Group	Normal Group	P Value
Area	11841.31 ± 3593.965	9980.08 ± 4446.192	**0.001**
Perimeter	440.113 ± 135.55	488.9615 ± 176.01	**0.006**
Major Axis	135.561 ± 24.99	136.437 ± 32.20	0.403
Minor Axis	112.856 ± 18.87	102.1329 ± 21.13	**0.001**
Contrast	0.5187 ± 0.16386	0.45821 ± 0.2016	**0.004**
Correlation	0.04942 ± 0.07420	0.05880 ± 0.07176	0.150
Energy	0.93279638619082 ± 0.055470128558995	0.907097610454514 ± 0.073988539113432	**0.001**
Homogenity	0.977876709669472 ± 0.014199141245954	0.9715907305283 ± 0.018537556863547	**0.001**
Mean	0.005598532042559 ± 0.001330400938078	0.005076366194382 ± 0.001742912032478	**0.004**
Std_Dev	0.080913565632421 ± 0.000082299063639	0.081123586817564 ± 0.001284612355464	**0.032**
Entropy	0.816509173331843 ± 1.075327506447608	1.320712859933843 ± 1.440804329246499	**0.001**
RMS	0.081110710565381 ± 6.7305E-17	0.081293460408549 ± 0.001289095360592	0.054
Variance	0.006577481015582 ± 0.000004979648033	0.006605410088042 ± 0.000221755979833	0.076
Smoothness	0.966779695512669 ± 0.011280772056419	0.957361611939308 ± 0.045084999562145	**0.011**
Kurtosis	105.13888931592825 ± 56.98548701322842	86.98114609165879 ± 64.61052742432929	**0.008**
Skewness	8.589997283628007 ± 4.603525504592328	7.107714805270727 ± 5.253714597114897	**0.008**

$$T_p = \sum_{i=1}^{N} [(Segment_{img}(i) = 1) \& (GroundTruth_{img}(i) = 1)] \quad (10)$$

$$T_N = \sum_{i=1}^{N} [(Segment_{img}(i) = 0) \& (GroundTruth_{img}(i) = 0)] \quad (11)$$

$$F_p = \sum_{i=1}^{N} [(Segment_{img}(i) = 1) \& (GroundTruth_{img}(i) = 0)] \quad (12)$$

$$F_N = \sum_{i=1}^{N} [(Segment_{img}(i) = 0) \& (GrountTruth_{img}(i) = 1)] \quad (13)$$

The proportion of TP outcomes to the total of TP and FN results is represented by recall and sensitivity, which are both equal. Sensitivity, thus, is a measure of how often the positive predictions come true or are accurate. Specificity is a measure of how often negative forecasts turn out to be accurate. Obtaining 100% specificity in

the medical field is unacceptable. The model's capacity to make accurate predictions can be assessed using accuracy as a performance criterion. The ratio of the TP value to the total positive value is shown by precision and the positive predicted value (PPV). Another performance metric that takes both sensitivity and specificity into account is the F1 score. It employs recall and precision to find the cases that were erroneously categorized. The performance of the binary classification model is evaluated using the AU. All the above-discussed performance measures are shown below, from (14) to (19).

$$Accuracy = \frac{TP + TN}{TP + FP + FN + TN} \times 100\% \tag{14}$$

$$TPR = Sensitivity = Recall = \frac{TP}{TP + FN} \times 100\% \tag{15}$$

$$Specificity = \frac{TN}{FP + TN} \times 100\% \tag{16}$$

$$Precision = PPV = \frac{TP}{TP + FP} \times 100\% \tag{17}$$

$$F1\,Score = 2\left(\frac{Precision \times Recall}{Precision + Recall}\right) \tag{18}$$

$$Area\ under\ curve(AUC) = \frac{1}{2}\left(\frac{TP}{TP + FN} + \frac{TN}{FP + TN}\right) \tag{19}$$

5 RESULTS AND DISCUSSION

The discussion here is about the findings of the experiments on the categorization of leukemia cancer. To create a leukemia detection system for the ALLIDB2 dataset, novel machine learning classification algorithms were used. This includes DT, KNN, RF, NN, and SVM. The Orange data analytics tool is used to develop the categorization model, as shown in Figure 5. The confusion matrix for five different classifiers is analyzed and shown in Figure 6. The test data was used for evaluation. To improve the efficiency of the classification process, the data is normalized in the range between 0 and 1. The normalization approach is the Min-Max method, as seen in (20).

$$x' = \frac{x_i - x_{min}}{x_{max} - x_{min}} \tag{20}$$

The normalized data is denoted by x', the input value is denoted by x_i, the lowest number in the input set is denoted by x_{min}, and the greatest number in the input set is denoted by x_{max}. Following the normalization phase, missing data is assigned values. Preprocessing and feature selection are then followed by the training-test data distribution stage. The 10-layered cross-validation approach is utilized in this phase. The following stage involved classification activities. Experiments with five different classification methods were carried out. The Random Forest method has been designed with a total of ten trees. The NN approach uses 100 hidden layer neurons, the hidden layer activation function ReLu, Adam as the optimizer, 200 iterations, and 0.001 as the learning rate. The radial basis function (RBF) is employed as the kernel in the SVM method, with a cost value of 1 and a regression loss of 0.10. The k-value in the kNN algorithm is set to 5 with Euclidean distance metrics.

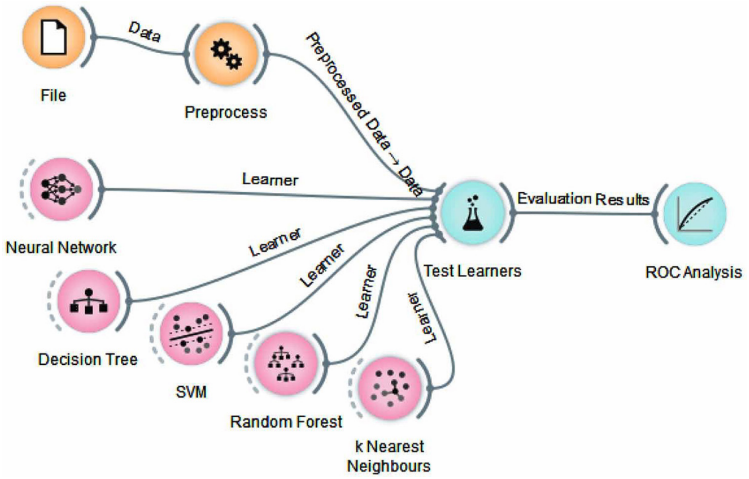

Fig. 5. Orange data analytic tools for five classification models

Finally, statistical evaluation criteria were utilized to test the effectiveness of the suggested model. A variety of evaluation approaches, including accuracy rate, sensitivity, specificity, and area under the ROC curve, have been used at this stage. Table 4 shows the findings achieved by using the proposed method. It provides a comparative analysis of various classification systems. From the table, it is clear that ANNs achieve a maximum accuracy value of 95%. The kNN algorithm achieves the second-greatest accuracy of 93.8%. The SVM algorithm achieves the lowest accuracy rating of 85.8%. Along with the accuracy rate, ANNs often produce higher outcomes in other statistical parameters. The Random Forest algorithm produces better results solely for sensitivity and NPV, which are 94.30% and 94.61%, respectively. At this point, AUC curves have been used. Figure 7 depicts the obtained AUC curves. When the figure is inspected, it is clear that ANNs (AUC: 0.989) and Random Forests (AUC: 0.973) have the highest area value under ROC. The DT technique produced the lowest results (AUC: 0.891). Table 5 compares important contributions made by researchers in the past where ANN was utilized for WBC categorization.

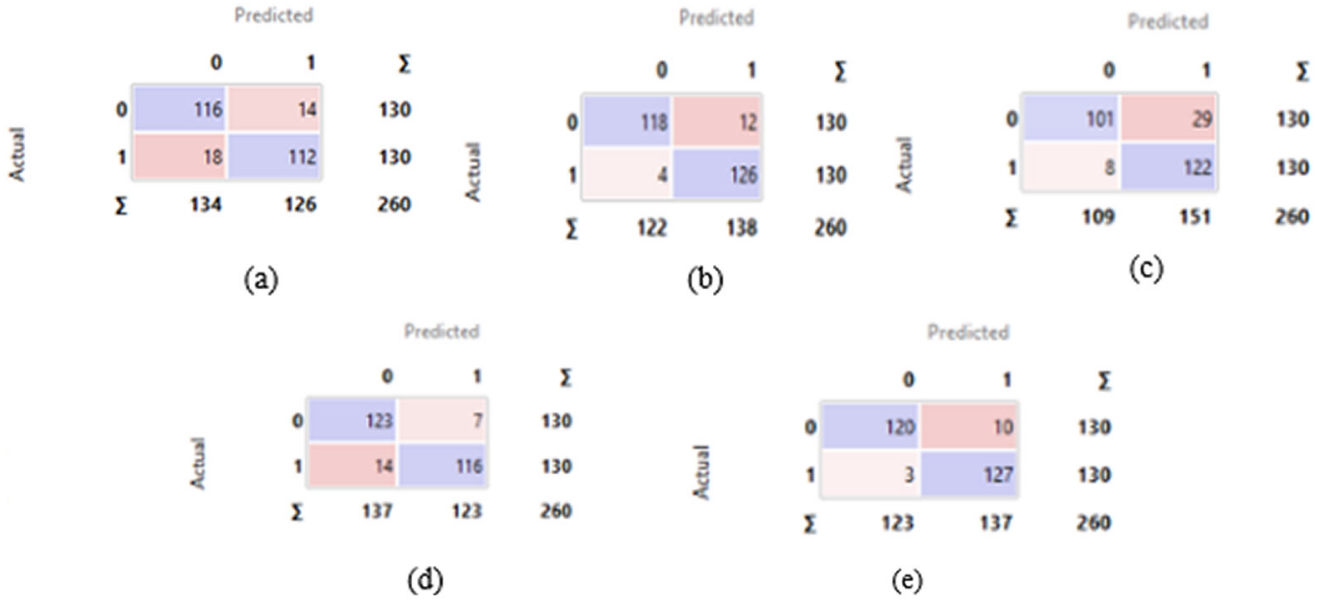

Fig. 6. Confusion matrix for DT, KNN, SVM, RF, and NN

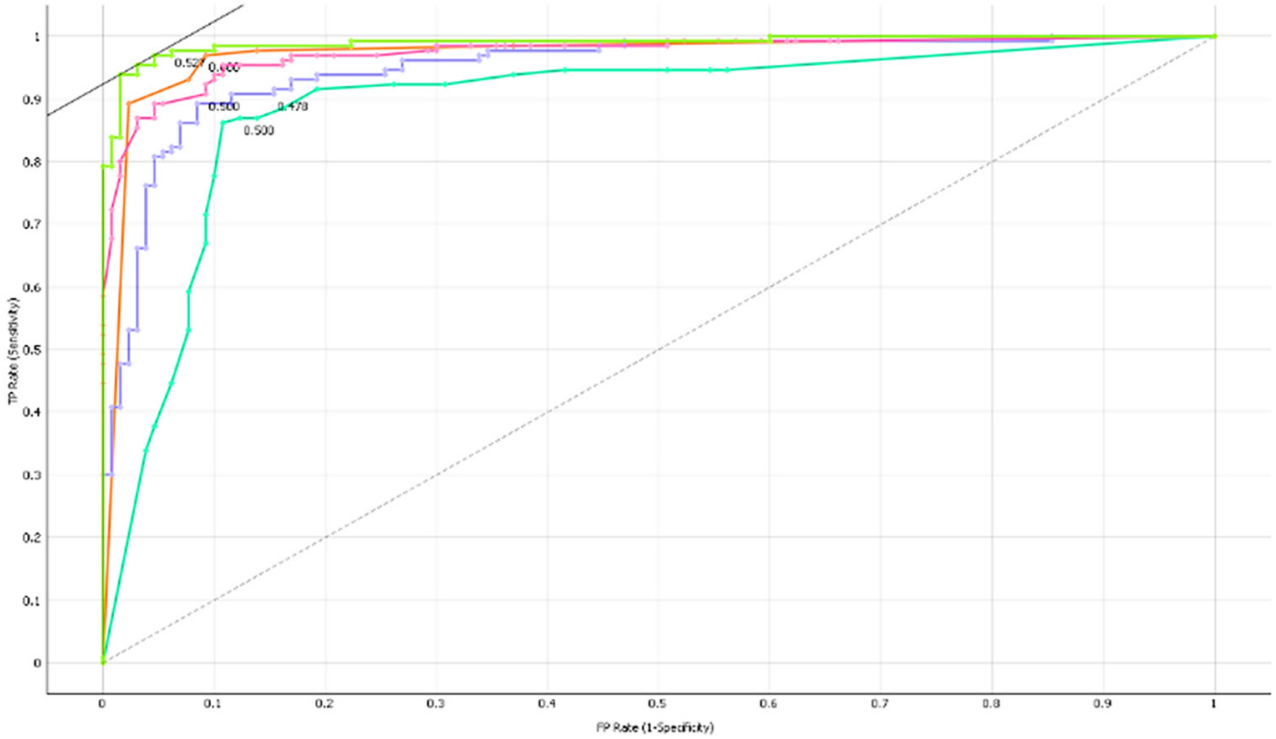

Fig. 7. AUC curve for all classifiers

Table 4. Comparative analysis of different classifiers

Algorithm	CA	Sensitivity	Specificity	F1	Precision	PPV%	NPV%	Recall	AUC
KNN	0.938	0.9130	0.9672	0.938	0.940	0.9692	0.9076	0.938	0.971
SVM	0.858	0.8079	0.9266	0.857	0.867	0.9384	0.7769	0.858	0.949
Random Forest	0.919	0.9430	0.8978	0.919	0.920	0.8923	0.9461	0.919	0.973
Neural Network	**0.950**	**0.9270**	**0.9756**	**0.950**	**0.951**	**0.9769**	**0.9230**	**0.950**	**0.989**
Decision Tree	0.877	0.8899	0.8656	0.877	0.877	0.8615	0.8923	0.877	0.891

Table 5. Result of proposed work compared with other existing methods

Research	Contribution	Application
Lee, H. & Chen, Y.P.P. [52]	Red blood cell segmentation, separation of overlapping cells, and hybrid neural network-based classifiers are used to identify red blood cells as normal or abnormal with 91% accuracy.	RBC classification system
Rawat, Jyoti, et al. [53]	WBC nucleus segmentation using k-means clustering, and an ensemble artificial neural network (EANN) is trained to classify WBCs into its five sub-classes with an accuracy of 95%.	Computer-aided system for WBCs classification in microscopic blood images.
Nazlibilek, Sedat, et al. [54]	An autonomous segmentation, classification, and counting system for WBCs that uses a neural network classifier with 95% accuracy using PCA.	ANN-based WBCs classification
Sadeghian, F., et al. [55]	WBCs are segmented using the active contour technique, and ANN is used to categorize WBCs into their five sub-classes with an accuracy of 78% for cytoplasm and 92% for nucleus segmentation.	Computer-aided diagnosis system for WBCs classification
Proposed Method	Segmentation of WBC cells is achieved using a concavity-based segmentation approach. The cells are categorized based on their morphological and statistical features using a Neural network as one of the classification approaches.	Computer-aided automatic diagnosis system for segmentation and classification of ALL BSIs.

6 CONCLUSION

Leukemia is a deadly ailment that impacts the WBCs and bone marrow, weakening the immune system. The traditional manual procedures for detecting leukemia are a complete blood count (CBC) and an examination of BSIs under a microscope. These approaches have imperfections and are laborious. The technological advancement is the reason that hundreds of automated procedures for computer-aided systems have been advocated for leukemia diagnosis. As a result, the life of the individual can be saved if he receives timely treatment. Computer-aided technologies have the capacity to substitute for conventional leukemia diagnosis. Pre-processing and segmentation are critical phases in the identification and classification of leukemia. Classifier accuracy relies heavily on it. As a result, researchers should suggest more effective pre-processing and segmentation techniques that work effectively for very noisy images and segment the blast cells with greater precision, resulting in higher leukemia classification accuracy. In this work, the selection of 12 statistically examined attributes exhibited an excellent capacity to discriminate between malignant and healthy blood cells. These characteristics were derived from 260 WBCs segmented from the ALL-IDB2 dataset. Five widely employed machine learning-based classifiers were chosen to accomplish the classification process.

The NN model performed better, with an AUC of 98.9% and an overall accuracy of 95%. Based on its accuracy, we recommend utilizing the NN model to distinguish between each category of acute leukemia cells. It has been noted that our proposed method performs on par with or better than previous contributions in a similar field. The findings inspire further research towards developing a reliable segmentation method that is independent of the stains employed in BSIs. If data accessibility is limited, specific techniques must be offered to produce impressive outcomes. Extending the data's training set, in particular, would prevent overfitting and boost the possibility of classification. The findings of this study suggest that future research should focus on developing a more robust segmentation algorithm. Furthermore, researchers should concentrate on enhancing classification probabilities and minimizing erroneous classification due to FN results. Such a device might potentially be employed as a health assistance device, facilitating manual examination and saving a significant amount of time.

7 REFERENCES

[1] S. Angelescu, N. M. Berbec, A. Colita, D. Barbu, and A. R. Lupu, "Value of multifaced approach diagnosis and classification of acute leukemias," *Maedica*, vol. 7, no. 3, pp. 254–260, 2012.

[2] N. Y. Asaad and M. Dawoud, "Diagnosis and prognosis of B-cell chronic lymphocytic leukemia/small lymphocytic lymphoma (BCLL/SLL) and mantle cell lymphoma (MCL)," *J. Egypt. Nat. Cancer Inst.*, vol. 17, no. 4, pp. 279–290, 2005.

[3] Hematology, "The American Society of Hematology," hematology.org, Accessed: Oct. 2020. [Online]. Available: https://www.hematology.org/

[4] Harvard Health Publishing. "What is Leukemia?" health.harvard.edu. Accessed: Oct. 4, 2020. [Online]. Available: https://www.health.harvard.edu/cancer/leukemia

[5] F. Xing and L. Yang, "Robust nucleus/cell detection and segmentation in digital pathology and microscopy images: A comprehensive review," *IEEE Reviews in Biomedical Engineering*, vol. 9, pp. 234–263, 2016. https://doi.org/10.1109/RBME.2016.2515127

[6] J. Wen, Y. Xu, Z. Li, Z. Ma, and Y. Xu, "Inter-class sparsity based discriminative least square regression," *Neural Networks*, vol. 102, pp. 36–47, 2018. https://doi.org/10.1016/j.neunet.2018.02.002

[7] O. M. Al-hazaimeh, A. A. Abu-Ein, N. M. Tahat, M. M. A. Al-Smadi, and M. M. Al-Nawashi, "Combining artificial intelligence and image processing for diagnosing diabetic retinopathy in retinal fundus images," *International Journal of Online & Biomedical Engineering*, vol. 18, no. 13, pp. 131–151, 2022. https://doi.org/10.3991/ijoe.v18i13.33985

[8] R. Sharma and R. Kumar, "A novel approach for the classification of leukemia using artificial bee colony optimization technique and back-propagation neural networks ICCCN 2018," in *Proc. 2nd Int. Conf. Commun., Comput. Netw.* Chandigarh, India: NITTTR, 2019, vol. 46, pp. 685–694. https://doi.org/10.1007/978-981-13-1217-5_68

[9] T. M. Khan, A. Robles-Kelly, and S. S. Naqvi, "A semantically flexible feature fusion network for retinal vessel segmentation," in *Neural Information Processing, 27th International Conference, ICONIP 2020,* Bangkok, Thailand, Springer International Publishing, Switzerland, 2020, vol. 1332, pp. 159–167. https://doi.org/10.1007/978-3-030-63820-7_18

[10] T. M. Khan, M. Alhussein, K. Aurangzeb, M. Arsalan, S. S. Naqvi, and S. J. Nawaz, "Residual connection-based encoder decoder network (RCED-Net) for retinal vessel segmentation," *IEEE Access*, vol. 8, pp. 131257–131272, 2020. https://doi.org/10.1109/ACCESS.2020.3008899

[11] M. Tabassum, T. M. Khan, M. Arsalan, S. S. Naqvi, M. Ahmed, H. A. Madni, and J. Mirza, "CDED-Net: Joint segmentation of optic disc and optic cup for glaucoma screening," *IEEE Access*, vol. 8, pp. 102733–102747, 2020. https://doi.org/10.1109/ACCESS.2020.2998635

[12] M. A. Alsalem *et al.*, "A review of the automated detection and classification of acute leukaemia: Coherent taxonomy, datasets, validation and performance measurements, motivation, open challenges and recommendations," *Comput. Methods Programs,* vol. 158, pp. 93–112, 2018. https://doi.org/10.1016/j.cmpb.2018.02.005

[13] T. A. Soomro, M. A. U. Khan, J. Gao, T. M. Khan, and M. Paul, "Contrast normalization steps for increased sensitivity of a retinal image segmentation method," *J. Signal Image Video Process*., vol. 11, no. 8, pp. 1509–1517, 2017. https://doi.org/10.1007/s11760-017-1114-7

[14] L. Putzu, G. Caocci, and C. D. Ruberto, "Leucocyte classification for leukaemia detection using image processing techniques," *Artif. Intell. Med*., vol. 62, no. 3, pp. 179–191, 2014. https://doi.org/10.1016/j.artmed.2014.09.002

[15] S. Chuprat, "Segmentation and detection of acute leukemia using image processing and machine learning techniques," *A review AUS*, vol. 26, pp. 511–531, 2019.

[16] K. Naveed, F. Abdullah, H. A. Madni, M. A. U. Khan, T. M. Khan, and S. S. Naqvi, "Towards automated eye diagnosis: An improved retinal vessel segmentation framework using ensemble block matching 3D filter," *Diagnostics*, vol. 11, no. 1, p. 114, 2021. https://doi.org/10.3390/diagnostics11010114

[17] T. Zuva, O. O. Olugbara, S. O. Ojo, and S. M. Ngwira, "Image segmentation, available techniques, developments and open issues," *Canadian Journal on Image Processing and Computer Vision*, vol. 2, no. 3, pp. 20–29, 2011.

[18] K. Kim, J. Jeon, W. Choi, P. Kim, and Y. S. Ho, "Automatic cell classification in human's peripheral blood images based on morphological image processing," in *AI 2001: Advances in Artificial Intelligence,* Springer, Berlin Heidelberg, Australia, 2001, vol. 2256, pp. 225–236. https://doi.org/10.1007/3-540-45656-2_20

[19] Q. Chen, X. Yang, and E. M. Petriu, "Watershed segmentation for binary images with different distance transforms," in *Proceedings of the 3rd IEEE International Workshop on Haptic, Audio and Visual Environments and Their Applications, HAVE 2004,* Ottawa, Ontario, Canada, 2004, pp. 111–116.

[20] N. Gharaibeh, A. A. Abu-Ein, O. M. Al-hazaimeh, K. M. Nahar, W. A. Abu-Ain, and M. M. Al-Nawashi, "Swin Transformer-based segmentation and multi-scale feature pyramid fusion module for alzheimer's disease with machine learning," *International Journal of Online & Biomedical Engineering*, vol. 19, no. 4, pp. 22–50, 2023. https://doi.org/10.3991/ijoe.v19i04.37677

[21] R. D. Labati, V. Piuri, and F. Scotti. *ALL-IDB (Acute Lymphoblastic Leukemia Image Database for Image Processing)*. Accessed: Oct. 2016. [Online]. Available: https://homes.di.unimi.it/scotti/all/download

[22] American Society of Hematology. *ASH-DATASET*. Accessed: Oct. 2020. [Online]. Available: http://imagebank.hematology.org/

[23] K. Naveed, F. Abdullah, H. A. Madni, M. A. U. Khan, T. M. Khan, and S. S. Naqvi, "Towards automated eye diagnosis: An improved retinal vessel segmentation framework using ensemble block matching 3D Filter," *Diagnostics*, vol. 11, no. 1, p. 114, 2021. https://doi.org/10.3390/diagnostics11010114

[24] M. Mehmood, T. M. Khan, M. A. Khan, S. S. Naqvi, and W. Alhalabi, "Vessel intensity profile uniformity improvement for retinal vessel segmentation," *Procedia Comput. Sci.*, vol. 163, pp. 370–380, 2019. https://doi.org/10.1016/j.procs.2019.12.119

[25] V. Acharya and P. Kumar, "Detection of acute lymphoblastic leukemia using image segmentation and data mining algorithms," *Med. Biol. Eng. Comput.*, vol. 57, no. 8, pp. 1783–1811, 2019. https://doi.org/10.1007/s11517-019-01984-1

[26] R. Labati, V. Piuri, and F. Scotti, "All-IDB: The acute lymphoblastic leukemia image database for image processing," in *2011 18th IEEE International Conference on Image Processing*, 2011, pp. 2045–2048. https://doi.org/10.1109/ICIP.2011.6115881

[27] V. Khobragade, J. Nirmal, and S. Patnaik, "Concave point extraction: A novel method for WBC segmentation in all images," in *Machine Intelligence and Signal Processing: Proceedings of International Conference, MISP 2019*, Springer Singapore, 2020, pp. 113–124. https://doi.org/10.1007/978-981-15-1366-4_9

[28] S. Mishra, B. Majhi, P. K. Sa, and L. Sharma, "Gray level co-occurrence matrix and random forest based acute lymphoblastic leukemia detection," *Biomed. Signal Process. Control*, vol. 33, pp. 272–280, 2017. https://doi.org/10.1016/j.bspc.2016.11.021

[29] J. Rawat, A. Singh, H. S. Bhadauria, J. Virmani, and J. S. Devgun, "Classification of acute lymphoblastic leukaemia using hybrid hierarchical classifiers," *Multimedia Tools Appl.*, vol. 76, no. 18, pp. 19057–19085, 2017. https://doi.org/10.1007/s11042-017-4478-3

[30] A. Bodzas, "Diagnosis of malignant haematopoietic diseases based on the automation of blood microscopic image analysis," *Master's Thesis, Technical University of Ostrava*, Ostrava, CZ, 2019.

[31] M. K. Khazaaleh, M. A. Alsharaiah, W. Alsharafat, A. A. Abu-Shareha, F. A. Haziemeh, and M. M. Al-Nawashi, "Handling DNA malfunctions by unsupervised machine learning model," *Journal of Pathology Informatics*, vol. 14, p. 100340, 2023. https://doi.org/10.1016/j.jpi.2023.100340

[32] J. Rawat, H. S. Bhadauria, A. Singh, and J. Virmani, "Review of leukocyte classification techniques for microscopic blood images," in *Proc. 2nd Int. Conf. Comput. Sustain. Global Develop. (INDIACom)*, 2015, pp. 1948–1954.

[33] J. Li *et al.*, "Identification of leukaemia stem cell expression signatures through Monte Carlo feature selection strategy and support vector machine," *Cancer Gene Therapy*, vol. 27, no. 1, pp. 56–69, 2020. https://doi.org/10.1038/s41417-019-0105-y

[34] S. Kumar, A. L. Fred, H. A. Kumar, P. S. Varghese, and S. A. Jacob, "Segmentation of anomalies in abdomen CT images by convolution neural network and classification by fuzzy support vector machine," *Hybrid Machine Intelligence for Medical Image Analysis: Springer*, pp. 157–196, 2020. https://doi.org/10.1007/978-981-13-8930-6_7

[35] Y. Wang *et al.*, "Morphological segmentation analysis and texture-based support vector machines classification on mice liver fibrosis microscopic images," *Current Bioinformatics*, vol. 14, no. 4, pp. 282–294, 2019. https://doi.org/10.2174/1574893614666190304125221

[36] A. Lubis, P. Sihombing, and E. Nababan, "Analysis of accuracy improvement in K-Nearest neighbor using principal component analysis (PCA)," in *Journal of Physics: Conference Series*, 2020, vol. 1566, no. 1, p. 012062. https://doi.org/10.1088/1742-6596/1566/1/012062

[37] A. Gautam, P. Singh, B. Raman, and H. Bhadauria, "Automatic classification of leukocytes using morphological features and naïve Bayes classifier," in *2016 IEEE Region 10 Conference (TENCON)*, 2016, pp. 1023–1027. https://doi.org/10.1109/TENCON.2016.7848161

[38] H. Gao, X. Zeng, and C. Yao, "Application of improved distributed naive Bayesian algorithms in text classification," *The Journal of Supercomputing*, vol. 75, no. 9, pp. 5831–5847, 2019. https://doi.org/10.1007/s11227-019-02862-1

[39] E. Purwanti and E. Calista, "Detection of acute lymphocyte leukaemia using k-nearest neighbor algorithm based on shape and histogram features," in *Journal of Physics: Conference Series*, 2017, vol. 853, no. 1, p. 012011. https://doi.org/10.1088/1742-6596/853/1/012011

[40] M. B. Rajesh and S. Sathiamoorthy, "Classification of leukemia image using genetic based k-nearest neighbor (G-KNN)," *Asian Journal of Computer Science and Technology*, vol. 7, no. 2, pp. 113–117, 2018. https://doi.org/10.51983/ajcst-2018.7.2.1869

[41] E. S. Wiharto, S. Palgunadi, and Y. R. Putra, "Cells identification of acute myeloid leukemia AML M0 and AML M1 using K-nearest neighbour based on morphological images," in *2017 International Conference on Data and Software Engineering (ICoDSE)*, 2017, pp. 1–6. https://doi.org/10.1109/ICODSE.2017.8285851

[42] S. N. M. Safuan, M. R. M. Tomari, and W. N. W. Zakaria, "White blood cell (WBC) counting analysis in blood smear images using various color segmentation methods," *Measurement*, vol. 116, pp. 543–555, 2018. https://doi.org/10.1016/j.measurement.2017.11.002

[43] S. Mishra, B. Majhi, and P. K. Sa, "Texture feature-based classification on microscopic blood smear for acute lymphoblastic leukemia detection," *Biomedical Signal Processing and Control*, vol. 47, pp. 303–311, 2019. https://doi.org/10.1016/j.bspc.2018.08.012

[44] M. A. Mohammed *et al.*, "Decision support system for nasopharyngeal carcinoma discrimination from endoscopic images using artificial neural network," *The Journal of Supercomputing*, vol. 76, no. 2, pp. 1086–1104, 2020. https://doi.org/10.1007/s11227-018-2587-z

[45] R. B. Hegde, K. Prasad, H. Hebbar, B. M. K. Singh, and I. Sandhya, "Automated decision support system for detection of leukemia from peripheral blood smear images," *Journal of Digital Imaging*, vol. 33, pp. 361–374, 2020. https://doi.org/10.1007/s10278-019-00288-y

[46] J. Zhao, M. Zhang, Z. Zhou, J. Chu, and F. Cao, "Automatic detection and classification of leukocytes using convolutional neural networks," *Medical & Biological Engineering & Computing*, vol. 55, no. 8, pp. 1287–1301, 2017. https://doi.org/10.1007/s11517-016-1590-x

[47] M. C. Su, C. Y. Cheng, and P. C. Wang, "A neural-network-based approach to white blood cell classification," *The Scientific World Journal*, vol. 2014, 2014. https://doi.org/10.1155/2014/796371

[48] A. Şengür, Y. Akbulut, Ü. Budak, and Z. Cömert, "White blood cell classification based on shape and deep features," in *2019 International Artificial Intelligence and Data Processing Symposium (IDAP)*, 2019, pp. 1–4. https://doi.org/10.1109/IDAP.2019.8875945

[49] S. Tantikitti, S. Tumswadi, and W. Premchaiswadi, "Image processing for detection of dengue virus based on WBC classification and decision tree," in *13th International Conference on ICT and Knowledge Engineering (ICT & Knowledge Engineering)*, 2015, pp. 84–89. https://doi.org/10.1109/ICTKE.2015.7368476

[50] J. Prinyakupt and C. Pluempitiwiriyawej, "Segmentation of white blood cells and comparison of cell morphology by linear and naïve Bayes classifiers," *Biomedical Engineering Online,* vol. 14, no. 1, p. 63, 2015. https://doi.org/10.1186/s12938-015-0037-1

[51] O. M. Al-Hazaimeh, M. Al-Nawashi, and M. Saraee, "Geometrical-based approach for robust human image detection," *Multimedia Tools and Applications*, vol. 78, pp. 7029–7053, 2019. https://doi.org/10.1007/s11042-018-6401-y

[52] H. Lee and Y. P. P. Chen, "Cell morphology-based classification for red cells in blood smear images," *Pattern Recognition Letters,* vol. 49, pp. 155–161, 2014. https://doi.org/10.1016/j.patrec.2014.06.010

[53] J. Rawat, A. Singh, H. Bhadauria, J. Virmani, and J. S. Devgun, "Application of ensemble artificial neural network for the classification of white blood cells using microscopic blood images," *International Journal of Computational Systems Engineering,* vol. 4, nos. 2–3, pp. 202–216, 2018. https://doi.org/10.1504/IJCSYSE.2018.091407

[54] S. Nazlibilek, D. Karacor, T. Ercan, M. H. Sazli, O. Kalender, and Y. Ege, "Automatic segmentation, counting, size determination and classification of white blood cells," *Measurement,* vol. 55, pp. 58–65, 2014. https://doi.org/10.1016/j.measurement.2014.04.008

[55] F. Sadeghian, Z. Seman, A. R. Ramli, B. H. A. Kahar, and M.-I. Saripan, "A framework for white blood cell segmentation in microscopic blood images using digital image processing," *Biological Procedures Online,* vol. 11, no. 1, p. 196, 2009. https://doi.org/10.1007/s12575-009-9011-2

8 AUTHORS

Vandana S. Khobragade is an Assistant professor at Lokmanya Tilak College of Engineering, Mumbai University, and a research scholar at Rajiv Gandhi Institute of Technology, Mumbai. Her areas of interest are Biomedical Image Processing, Machine Learning, Deep Learning (E-mail: vandanakhobragade@ltce.in).

Jagannath H. Nirmal is Professor and HoD at K. J. Somaiya College of Engineering, Mumbai. His area of interest is audio-speech processing, Image Processing, Deep Learning, and Machine Learning (E-mail: jhnirmal@somaiya.edu).

Aayesha Hakim is an Assistant professor at K. J. Somaiya College of Engineering, Mumbai. Her areas of interest are Biomedical Image Processing, Machine Learning, Pattern Recognition, and its applications (E-mail: aayesha.hakim@gmail.com).